



Anisotropic wood–water interactions determined by gravimetric vapor sorption experiments

Antoni Sánchez-Ferrer · Max Engelhardt · Klaus Richter

Received: 11 January 2023 / Accepted: 9 February 2023 / Published online: 27 February 2023
© The Author(s) 2023

Abstract Gravimetric vapor sorption experiments were performed on beech wood samples to determine the directional permeability, diffusion and sorption coefficients in the three orthotropic wood directions. Dynamic Vapor Sorption (DVS) experiments allowed for the direct evaluation of the diffusion coefficient from the analysis of the kinetic sorption profile using a double stretched exponential model with values ranging from 0.10×10^{-10} to 1.52×10^{-10} m²/s and depending on the wood direction of the sample and the RH-values. Moisture sorption isotherms (MSIs) were constructed and fitted to a modified Guggenheim-Anderson-de Boer and a Sorption Site Occupancy model, which allowed for the calculation of the sorption coefficient which was found to be between 2.4 and 3.0 mol/(m³ Pa). Dynamic Vapor Transport (DVT) experiments were performed to calculate the permeability coefficient from the vapor flow rate and it ranges between 0.56×10^{-10} and 4.38×10^{-10} mol/

(m s Pa) as a function of the flow direction and RH conditions. These results indicate that such an experimental approach is suitable for determining wood–moisture interactions.

Keywords Vapor sorption · Vapor transport · Diffusivity · Permeability · Sorption · Wood

Introduction

Water transfer is one of the most important phenomena in wood processing, usage and storage. Wood moisture permeability and diffusivity are properties that determine how water molecules pass through and move within, respectively, bulk solids or porous network structures like wood due to differences in external or internal water concentration (Babbitt 1950; Siau 1984; Avramidis and Siau 1987; Skaar 1988). The amount of moisture that permeates through a barrier is related both to the sorption and diffusion coefficient ($P=D S$). The higher the diffusivity of the water molecules through the barrier, the higher will be the permeability. However, if moisture is highly sorbed in the barrier, then the barrier will be more permeable to water. Such properties have a direct effect on several timber technical processes, e.g., drying, steaming, soaking, solvent-exchange drying, boiling, surface treatment, chemical modification and impregnation (Lehringer et al. 2009; Panigrahi et al. 2018), as well as in the final quality of the wood products (Skaar

Supplementary Information The online version contains supplementary material available at <https://doi.org/10.1007/s10570-023-05093-z>.

A. Sánchez-Ferrer (✉) · M. Engelhardt · K. Richter
School of Life Sciences, Chair of Wood Science, Technical University of Munich, 80797 Munich, Germany
e-mail: sanchez@hfm.tum.de

M. Engelhardt
e-mail: engelhardt@hfm.tum.de

K. Richter
e-mail: richter@hfm.tum.de

1988; Ross 2010). Moisture permeability/diffusivity has been explored by many authors and reviewed by Hansmann et al. (2002), where factors like wood structure, anatomical directions, extractives content, and the influence of early/latewood, sap/heartwood and juvenile/mature wood have been studied in order to understand better the effect on the moisture–wood interactions that are directly connected to wood treatability (Choong and Fogg 1972). A recent review by Thybring et al. (2019) pointed out the need for new models for describing sorption processes that are affected by boundary conditions, cell wall diffusion, swelling/shrinkage and moisture-induced phase transitions in wood.

Several experimental approaches have been used for the determination of moisture permeability, e.g., hygrometric and vapor pressure manometric methods (Choong et al. 1974; Jinman et al. 1991; Glass 2007; Simo-Tagne et al. 2016). So far, no gravimetric technique—except those using the tedious and longish permeability cup experiments (Geving et al. 2000; Palanti et al. 2001)—has been used for such a purpose. Contrary to that, the gravimetric vapor sorption technique has a fully automated precise control of both the relative humidity and the temperature, and it monitors the mass sorption of the samples obtaining results in 1 to 5 days with a high accuracy level (Burnett 2006; Yu 2008).

From the gravimetric vapor sorption experiments, meaningful information can be obtained, e.g., vapor sorption kinetics, moisture sorption isotherms and water vapor transmission rates (Crank 1975; Piringir and Baner 2000). Sorption kinetics have been studied and evaluated (Siepmann and Peppas 2011; Negrini et al. 2014; Amini-Fazl and Mobedi 2020) following different models, e.g., Ritger and Peppas (1987), Weibull (Weibull 1951) and Peleg (Peleg 1988), but so far no full explanation of the experimental data has been achieved for wood samples. Moreover, moisture sorption isotherms have been modeled using several physical and empirical approaches (Kollmann 1963; Nelson 1983; Basu et al. 2006), and the most widely used models for explaining the wood behavior are the original (GAB) (Anderson 1946) and the modified Guggenheim, Anderson, de Boer models (GAB*) (Viollaz and Rovedo 1999). One of the models that better explain the wood–water interactions during sorption processes is the Sorption Site Occupancy (SSO) model (Willems 2014, 2015). Finally, lagtime

water vapor transmission experiments are an easy way to evaluate wood permeability and diffusivity (Al-Ismaily et al. 2012; Fuoco et al. 2020).

In this paper, we show how the moisture permeability (P) and diffusion (D) coefficients of wood in the three orthotropic directions can be calculated, as well as the sorption (S) coefficient, based on gravimetric vapor sorption experiments. On the one hand, the sorption kinetics was evaluated using Dynamic Vapor Sorption (DVS) experiments by fitting the experimental data to a Double Stretched Exponential (DSE) model. From these results, the Moisture Sorption Isotherm (MSI) was constructed and fitted to the modified GAB model for interpolation purposes, and the amount of bound and non-bound water molecules in the cell wall during the sorption processes was estimated by using a version of the SSO model. On the other hand, the lagtime experiments using Dynamic Vapor Transport (DVT) experiments were evaluated by fitting the experimental data to an exponential-linear fitting approach. Thereby, information on the diffusion and sorption coefficients and on the diffusion and permeability coefficients were directly obtained from the DVS and the DVT experiments, respectively, resulting in a corresponding entire picture of the wood–moisture interactions.

Experimental section

Materials

Beech wood (*Fagus sylvatica* L.) was used for this study. Three veneer disk samples of ca. 1 mm thickness and 12 mm diameter were cut perpendicular to the three wood orthotropic directions, i.e., disk1-L (longitudinal), disk2-R (radial) and disk3-T (tangential), for conducting both moisture sorption and transmission experiments (Fig. SI-1). Ultrapure water (Milli-Q water) and anhydrous CaCl₂ were used to create the inner 100% and 0% RH-values in the permeability setup, respectively, during moisture transmission experiments.

Dynamic vapor sorption (DVS) experiments

Moisture sorption or Dynamic Vapor Sorption (DVS) experiments were conducted using a gravimetric vapor sorption device (DVS Advantage ET, Surface

Measurement Systems). The device is equipped with a microbalance and a chamber that is purged with a nitrogen flow of 200 cm³/min (12 L/h) at a selected relative humidity (RH) value obtained by mixing different flows of dry and water-saturated nitrogen. Two aluminum-perforated pans were used for conducting these experiments placing the sample in one of them while using the other as a reference to eliminate sorption effects from the holders. After conditioning the sample at 23 °C and at 0% RH until complete dryness, the measurement starts by increasing the RH of the nitrogen flow in steps of 10% until 100% RH is reached (actually, *ca.* 96% RH). After reaching this final adsorption step, the RH-value is reduced in steps of 10% until 0% RH is reached, completing the cycle. The criterion for increasing/decreasing the set RH-value is a threshold in the variation in mass per unit time with respect to the initial dry mass to a value of $d(m/m_{dry})/dt < 0.001\%/min$ over 10 min, where at this point, the sample is measured for one extra hour prior to changing the RH for the next measuring step. With this stopping criteria, the measuring time is considerably reduced even though the obtained extrapolated equilibrium moisture content has an error of *ca.* 1%, and the kinetics appear to be *ca.* 20% faster compared to those from the $d(m/m_{dry})/dt = 0.0003\%/min$ stopping criteria (Glass 2007). During the measurement, the mass of the sample and the RH-value are recorded as a function of time.

Fitting the dynamic vapor sorption (DVS) experimental data

Each dynamic moisture sorption step was analyzed using a double stretched exponential (DSE) model—or double Weibull (W) model—and the Ritger-Peppas (RP) model for comparison. Single exponential (SE), double exponential (DE) and single stretched exponential (SSE) models were also used and discarded based on the analysis of the residues after fitting the data (Appendix 1). The DSE model has the following expression:

$$\frac{m}{m_{dry}} = \left(\frac{m}{m_{dry}} \right)_{eq} + A_1 e^{-\left(\frac{t-t_0}{\tau_1}\right)^{\beta_1}} + A_2 e^{-\left(\frac{t-t_0}{\tau_2}\right)^{\beta_2}} \quad (1)$$

where m/m_{dry} is the mass ratio with respect to the dry mass of the sample, $(m/m_{dry})_{eq}$ is the mass ratio at the infinite time, A_1 and A_2 , τ_1 and τ_2 , and β_1 and β_2 are

the amplitude, the lifetime and the stretched exponential factor of each single stretched exponential function, respectively.

From the fitting of each sorption step, an equivalent lifetime value τ and stretched exponential factor β can be obtained by applying a minimization process (Appendix 1) and converting these values into those of an equivalent SSE model. Therefore, the corresponding kinetic constant $k = 1/\tau$ and the diffusivity or diffusion coefficient D can be calculated (Neogi 1996) following the expression:

$$D = \pi \left(\frac{V}{2A} \right)^2 k \quad (2)$$

where V is the volume of the sample and A the total area exposed to sorption processes. In this way, the three anisotropic diffusion coefficients, i.e., D_L , D_R and D_T , can be obtained from the corresponding three beech disks—disk1-L, disk2-R, and disk3-T. It should be noted that this equation (Eq. 2) leads toward the calculation of apparent diffusion coefficient values since the mass transport resistance is considered negligible and the temperature is assumed to be locally constant.

Dynamic vapor transport (DVT) experiments

Moisture transmission or Dynamic Vapor Transport (DVT) experiments were conducted using the same DVS Advantage ET (Surface Measurement Systems) device as the one used for moisture sorption experiments. Two moisture transmission cups were used for conducting these experiments, each of which consisted of three 3D-printed components (Fig. SI-2). Both cups have a middle part with two male screws that close and seal the upper and bottom components. The upper component consists of an open cup of 7.8 mm diameter with an O-ring seal of 10.5 mm diameter for ensuring a good sealing of the system when mounting the sample. The bottom component consists of a cylindrical reservoir where water or a drying agent can be placed to generate a 100% or 0% RH condition, respectively, inside the moisture transmission cup. In the reference cup, a thin aluminum disk was placed, while in the measuring cup, a wood beech disk was inserted. Before running the experiments, the sample has to be equilibrated to the starting conditions in the DVS

chamber by using only the upper and middle parts of the moisture transmission cups—equilibrated to the outer RH-value and to 0% RH for the experiments using water and desiccant in the bottom part of the cup, respectively. Once the sample was equilibrated, the same amount of water—or drying agent—was placed in both bottom components of the moisture transmission cups, which were closed and placed in the DVS chamber allowing the moisture transmission experiment to start—for experiments using desiccant in the cup, the outer RH-value was raised to the set value. After some hours, when the mass profile shows a constant slope, the experiment was considered to be completed. During the measurement, the mass of the sample and the RH-value are recorded as a function of time.

Fitting the dynamic vapor transport (DVT) experimental data

The experimental data shows a mass profile with a starting plateau region that turns down towards a constant linear behavior when the RH-value inside the permeability cup is higher than that of the DVS chamber. When the inner RH-value is lower than the one from outside of the permeability cup, then a continuous mass increase is observed until reaching a constant rate. In order to evaluate both the initial (diffusivity) and final (permeability) process, the following fitting function was used:

$$\frac{m}{m_0} = 1 + M_w \left(e^{-\left(\frac{t-t_0}{\tau}\right)^\beta} - 1 \right) + \frac{\dot{m}}{m_0} (t - t_0) \quad (3)$$

where m/m_0 is the mass ratio with respect to the initial mass of the sample, M_w , τ and β are the amplitude or moisture capacity, the lifetime and the stretched exponential parameter of the diffusivity process, and \dot{m} is the slope—mass rate or flow rate—of the permeability process. Note that m refers to the initial mass of the sample plus the absolute value of the transferred water mass Δm ($m = m_0 + \Delta m$). Therefore, in order to normalize all experiments, $m/m_0 = 1$ at $t = 0$.

From the analysis of the data, the permeability coefficient P , the diffusion coefficient D , the transmission rate TR and the sorption coefficient

S following Henry's law can be calculated (Crank 1975; Piringer and Baner 2000).

$$P = \frac{l\dot{m}}{A\Delta p} \quad (4)$$

$$D = \pi \left(\frac{V}{2A} \right)^2 \frac{1}{\tau} \quad (5)$$

$$TR = \frac{\dot{m}}{A} \quad (6)$$

$$S = \frac{P}{D} \quad (7)$$

where l and A are the thickness and area of the sample at 0% RH, respectively, and Δp is the difference in water partial pressure.

A commonly used approach for the diffusion coefficient D determination in moisture transmission experiments is the one using the following expressions (Al-Ismaïly et al. 2012; Fuoco et al. 2020):

$$D = \frac{l^2}{6\theta} = \frac{l^2\dot{m}}{6m_0M_w} \quad (8)$$

where θ is the lagtime calculated from the crossing of the extrapolated linear permeability region at $m/m_0 = 1$ (linear approach) or $\theta = M_w/\dot{m}$ (exponential-linear approach).

Note that Eq. 4 allows for a simple calculation of the permeability coefficient when both the vapor diffusion resistance of the still air inside the DVT cup and the boundary layer resistance on the exterior of the DVT cup are considered negligible. Actually, the evaluation of the intrinsic permeability parameter (ISO 12572) shows deviations between 2 and 9%, 5% and 13%, and 28% and 32% for the tangential, radial and longitudinal directions, respectively. The mass transfer Biot number (Bi_m) along all RH-values is below the limit of 50, where the effect of the boundary layer resistance on the exterior cannot be neglected (Thorell and Wadsö 2018). Therefore, those two factors—the intrinsic permeability parameter and the mass transfer Biot number—should be considered when the calculation of more accurate permeability is required. Nonetheless, Eq. 4 is a good approximation to reality within the errors.

Results and discussion

Dynamic vapor sorption (DVS) experiments—diffusion coefficient (D) determination

Moisture sorption experiments were performed on the three beech disks in order to determine the moisture sorption isotherms and the water diffusivity along the three wood orthotropic directions, i.e., longitudinal (L)—disk1-L-, radial (R)—disk2-R—and tangential (T)—disk3-T.

From the mass ratio profile, the three beech disks (disk1-L, disk2-R and disk3-T) showed that the sorption process had a clear dependency on the wood direction perpendicular to the disk plane. Times for reaching the final RH-value in the adsorption (*ca.* 96% RH) and desorption (0% RH) process of $t_{\max} = 52$ h, 63 h and 60 h, and of $t_{\text{final}} = 112$ h, 132 h and 130 h, respectively (Fig. SI-3, SI-4 and SI-5). Thus, an evident difference is observed between the longitudinal direction—disk1-L—and the radial and tangential direction—disk2-L and disk-T—indicating a higher water diffusivity along the fiber direction; disk2-R and disk3-T require 18% and 16% more time than disk1-L, respectively.

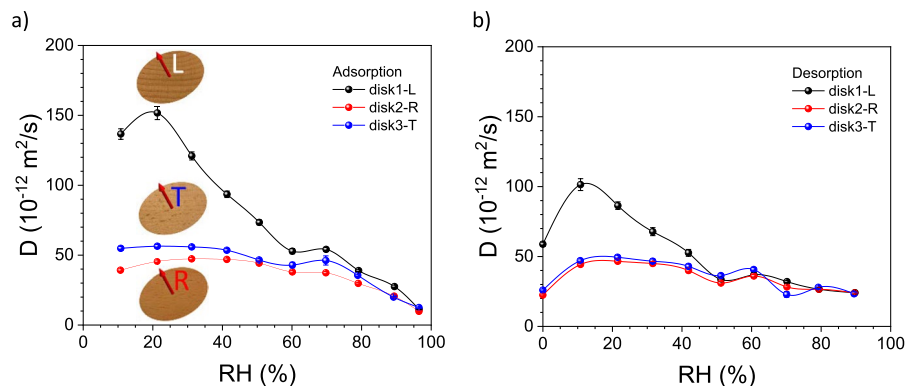
Each step of the moisture sorption experiment was analyzed by fitting the experimental data with a double stretched exponential (DSE) model (Fig. SI-3, SI-4 and SI-5, and Table SI-1, SI-2 and SI-3) and with the Ritger-Peppas (RP) model (Fig. SI-6, SI-7 and SI-8, and Table SI-4, SI-5 and SI-6). It has to be noted that the power-law RP model is an approximation to the DSE model and is only valid at the beginning of the sorption process. Details about these models can be found in Appendix 1, where the fitting functions and the corresponding evaluations are described. The

DSE model is the best model for explaining all experimental moisture sorption data compared to the use of a double exponential (DE) function—the two parallel exponential kinetics (PEK) model (Thybring et al. 2019; Zelinka et al. 2021)—or the single stretched exponential function—the Weibull model (Zeng and Xu 2017). Moreover, the DSE model allows for the extrapolation of the mass ratio at the infinite time ($m/m_{\text{dry}})_{\text{eq}}$ in a more accurate way, using this value for the precise construction of the moisture sorption isotherm (MSI). From the resulting fitting parameters, the sorption kinetic constant k and the corresponding diffusion coefficient D were evaluated using the DSE model (Fig. SI-3, SI-4 and SI-5, and Table SI-1, SI-2 and SI-3).

Figure 1 shows the diffusion coefficient obtained from the kinetic constant profiles when using the DSE model (Fig. SI-9) for the three beech disks in the adsorption and desorption process. The directional diffusion coefficient is between 1.52×10^{-10} and 0.11×10^{-10} m^2/s , between 0.47×10^{-10} and 0.10×10^{-10} m^2/s , and between 0.56×10^{-10} and 0.13×10^{-10} m^2/s for the longitudinal, radial and tangential direction, respectively. The diffusivity tends to decrease upon increasing the RH in the adsorption process and, vice versa in the desorption process. This behavior has previously been reported with values for the diffusion coefficient that decrease from 0.88×10^{-10} to 0.06×10^{-10} m^2/s when increasing the RH from 5 to 80% RH (Majka et al. 2022), and similar to other published results obtained from different methods (Olek et al. 2005; Simo-Tagne et al. 2016; Gezici-Koç et al. 2017).

Comparing the adsorption to the desorption profile, hysteresis in the diffusivity is observable at low RH-values. This could be explained by the change

Fig. 1 a Adsorption and b desorption diffusion coefficient (D) for the three beech disks obtained using the DSE model



in the conformation of the water-binding polymers (Vrentas and Vrentas 1996), i.e., hemicelluloses and amorphous cellulose, in the wood structure during the desorption process, which might hinder the diffusion of the water molecules through the solid matrix.

Comparing the results from those using the RP model, a discrepancy is observed that can be attributed to the fact that only the data covering the 40% of the total sorption are evaluated with this model (Appendix 1)—only the very first mass change in the adsorption/desorption process can be evaluated. To visualize these trends better, the adsorption/desorption diffusion coefficient obtained from the DSE model, the RP model, and the equivalent to the SSE exponential function from the RP model for the three beech disks at different relative humidity values are shown in Fig. SI-10. The tendencies look the same between models with DSE/RP ratio values of 1.47 ± 0.15 (average \pm standard deviation) and 0.97 ± 0.07 and with DSE/SSE ratio values of 0.97 ± 0.07 and 0.88 ± 0.10 in the adsorption and desorption diffusivity values, respectively. This indicates that both the DSE and the SSE approaches are comparable, the first one being more accurate because it is taking into account all sorption experimental points.

The relative directional kinetic constant (k_{rel}) and diffusion coefficient (D_{rel}) between the three wood orthotropic directions were also evaluated as shown in Fig. SI-11. From this evaluation, the L-direction is the one showing the highest diffusion coefficient, followed by the T-direction and, finally, by the R-direction ($L > T \geq R$) with ratio values ranging from 3.5 to 1.0 (L/R), from 2.7 to 1.0 (L/T) and from 0.72 to 1.0 (T/R) at low and high RH-values, respectively. This corresponds to average L/R ratio values of 2.0 ± 0.9 and 1.5 ± 0.6 , average L/T ratio values of 1.6 ± 0.6 and 1.4 ± 0.5 and average R/T ratio values of 0.9 ± 0.1 and 1.0 ± 0.1 in the adsorption and desorption absolute orthotropic diffusion values, respectively; similar ratios were obtained for the kinetic constants. Finally, the average directional diffusion coefficient for the three beech disks was calculated and the values were $\overline{D}_L = 7.6 \pm 4.8 \times 10^{-11}$ and $5.2 \pm 2.7 \times 10^{-11}$ m²/s, $\overline{D}_R = 3.6 \pm 1.2 \times 10^{-11}$ and $3.4 \pm 0.9 \times 10^{-11}$ m²/s, and $\overline{D}_T = 4.2 \pm 1.5 \times 10^{-11}$ and $3.6 \pm 1.1 \times 10^{-11}$ m²/s during the adsorption and desorption processes, respectively. All single diffusion coefficient values for the three beech disks can be found in Table SI-1, SI-2 and SI-3.

Moisture Sorption Isotherms (MSI)—Sorption coefficient (S) determination

The sorption behavior of the beech samples was studied upon constructing the corresponding Moisture Sorption Isotherms (MSIs), and the results were compared between them. MSI curves were constructed by taking the extrapolated mass ratio at the infinite time ($m/m_{dry,eq}$) from the fitting of each sorption step using the DSE model (Table SI-1, SI-2 and SI-3). Then, each MSI curve was fitted using the modified Guggenheim-Anderson-de Boer (GAB*) model (Viollaz and Rovedo 1999; Sandoval et al. 2011). Moreover, the hysteresis factor η could be obtained by calculating the area ratio between the desorption and adsorption isotherms. The number of bounded and non-bounded water molecules was evaluated using a modified version of the Sorption Site Occupancy (SSO) model (Freundlich 1906; Willems 2014, 2015) after the deconvolution of the MSI. In this new approach, the bound water moisture capacity profile (M_{SSO}) was obtained by using a power-law function and fitting the data up to the critical water activity value a_w^* ($0 < a_w < a_w^*$). The non-bound water moisture capacity profile was obtained by subtracting the M_{SSO} profile from the MSI. Appendix 2 shows all details concerning the MSI fitting models and the parameters obtained from the experimental data.

Figure SI-12 shows the moisture sorption isotherm with the corresponding fitting curve following the GAB* model ($0 \leq a_w \leq 0.99$) (Viollaz and Rovedo 1999; Sandoval et al. 2011), together with its deconvolution into the bound and non-bound water moisture capacity for the three beech disks. Moreover, all fitting parameters and derived properties are summarized in Table SI-7. The results from the SSO model analysis indicate a good agreement with previous works (Willems 2014, 2015), where the exponent obtained from the power-law function is $\bar{n} = 0.83 \pm 0.01$, the maximum bound water moisture capacity is $\overline{M}_{SSO}^0 = 0.134 \pm 0.009$ and the sorption sites' molar concentration $\overline{SSO} = 7.5 \pm 0.3$ mmol/g—close to the values obtained by other techniques (Gezici-Koç et al. 2017; Grönquist et al. 2019; Thybring et al. 2020, 2021). Finally, the hysteresis factor η was evaluated for the three beech samples with an average value of $\bar{\eta} = 1.26 \pm 0.02$.

From the MSI curves, the sorption coefficient (S) can be calculated (Appendix 2) taking

into account the moisture content ($\Delta m/m_{\text{dry}}$), the partial vapor pressure (p) and the volume of the sample (V), which changes as a function of the RH. Figure SI-13 shows the sorption coefficient profile for the three beech samples in the adsorption and desorption process. These curves were used to estimate the average sorption coefficient value and, when combined with the permeability coefficient values, to determine the diffusion coefficient ($D=P/S$) indirectly. The average sorption coefficient for the three directions was $\bar{S}_L = 2.3 \pm 0.5$ and 3.0 ± 0.4 mol/(m³ Pa), $\bar{S}_R = 2.7 \pm 0.6$ and 3.4 ± 0.4 mol/(m³ Pa) and $\bar{S}_T = 2.1 \pm 0.5$ and 2.7 ± 0.3 mol/(m³ Pa) in the adsorption and desorption processes, respectively, which do not differ that much from the initial sorption coefficient values calculated using the gas-polymer-matrix model (Raucher and Sefcik 1983)— $\bar{S}_{L0} = 3.2$ and 4.5 mol/(m³ Pa), $\bar{S}_{R0} = 2.7$ and 4.1 mol/(m³ Pa) and $\bar{S}_{T0} = 2.5$ and 3.4 mol/(m³ Pa). From the sorption coefficients out of the three beech disks, the corresponding adsorption and desorption average sorption coefficients were calculated $\bar{S}_{\text{ads}} = 2.4 \pm 0.6$ mol/(m³ Pa) and $\bar{S}_{\text{des}} = 3.0 \pm 0.6$ mol/(m³ Pa). All single sorption coefficient values for the three beech disks can be found in Table SI-8. The gas-polymer-matrix model assumes a non-linear Henry's law behavior of the gas molecules because of interactions with the glassy polymers in the matrix, which modify the mobility of the polymer backbones.

With both the diffusion and the sorption coefficients at a certain RH-value, the permeability coefficient could be estimated as the product of these two coefficients— $P(\text{RH})=D(\text{RH}) S(\text{RH})$ —and, therefore, the corresponding average value. Even though the experiment is not strictly a transmission process where water flows through the sample with a certain amount of water retained—but rather a diffusion process, where water either accumulates (adsorption) or leaves (desorption) the sample—a prediction for the permeability coefficient was obtained. The results show directional average permeability coefficient values of $\bar{P}_L = 1.7 \pm 1.0 \times 10^{-10}$ mol/(m s Pa), $\bar{P}_R = 8.9 \pm 2.4 \times 10^{-11}$ mol/(m s Pa), and $\bar{P}_T = 8.3 \pm 2.5 \times 10^{-11}$ mol/(m s Pa), which can be used as an estimation.

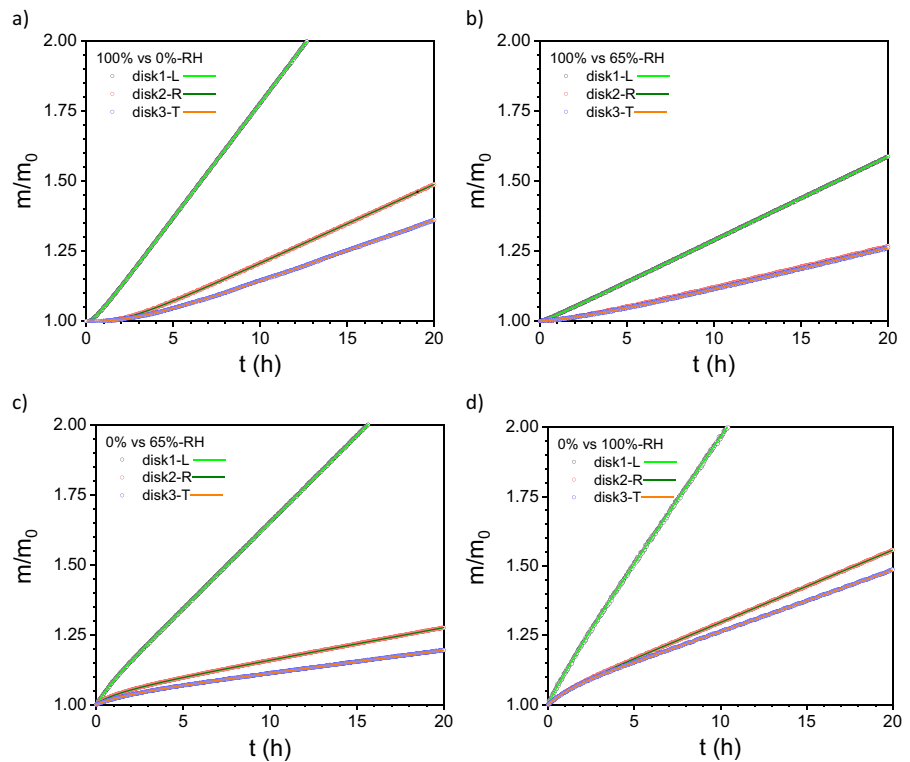
Dynamic vapor transport (DVT) experiments—permeability (P) and diffusion (D) coefficient determination

In order to determine the water permeability in the three orthotropic directions of wood, lagtime experiments—Dynamic Vapor Transport (DVT) experiments—were conducted using newly designed permeability cups (Fig. SI-2). In the upper part, the sample is attached between two O-ring seals and, in the bottom part, either pure water or a drying agent is placed to create 100% or 0% RH, respectively, inside the cup. Both parts are assembled by a double-male screw component, which seals the cup. In Fig. 2, permeability experiments on the three beech disks with the water transmission parallel to the longitudinal (L), radial (R), and tangential (T) directions at different relative humidity conditions are shown.

Two different experimental conditions were studied: (i) DVT experiments placing water in the bottom component of the cup—100% RH—were conducted against 0% and 65% RH of the outer gas flow; and (ii) DVT experiments placing drying agent in the bottom component of the cup—0% RH—were conducted against 65% and 100% RH of the outer gas flow. For the first set of experiments, water molecules are adsorbed on the surface of the wood sample exposed to the inner part of the cup with almost no change in the measured mass. For the second set of experiments, water molecules are adsorbed on the surface of the wood sample exposed to the outer gas flow part of the cup with an immediate increase in the mass. Then, water molecules start to diffuse through the sample—transient state or diffusive state—(i) without any loss of mass because water molecules are kept in the cup-sample system, or (ii) with a continuous gain of moisture because water molecules are incorporated in the cup-sample system. Once the water molecules reach the opposite surface of the wood sample, the desorption process takes place (i) with the corresponding loss of mass, or (ii) with the corresponding gain of mass. At this point, the system losses/gains mass and approaches a constant mass change rate (steady-state or permeation state) (Fig. SI-14). As a result, a convex shape (Fig. 2a and b) is obtained after conditioning the sample to the outer RH-value—0% or 65% RH—and a concave shape (Fig. 2c and d) after being conditioned to inner conditions—0% RH.

Using the exponential-linear fitting approach indicated in the Experimental Section, both the diffusion

Fig. 2 Permeability experiments on the three beech disks under different conditions: inner RH-value of 100% against outer RH-value of **a** 0% and **b** 65%; inner RH-value of 0% against outer RH-value of **c** 65% and **d** 100%. The lines are the fits to the experimental data using the exponential-linear fitting function (Eq. 4)



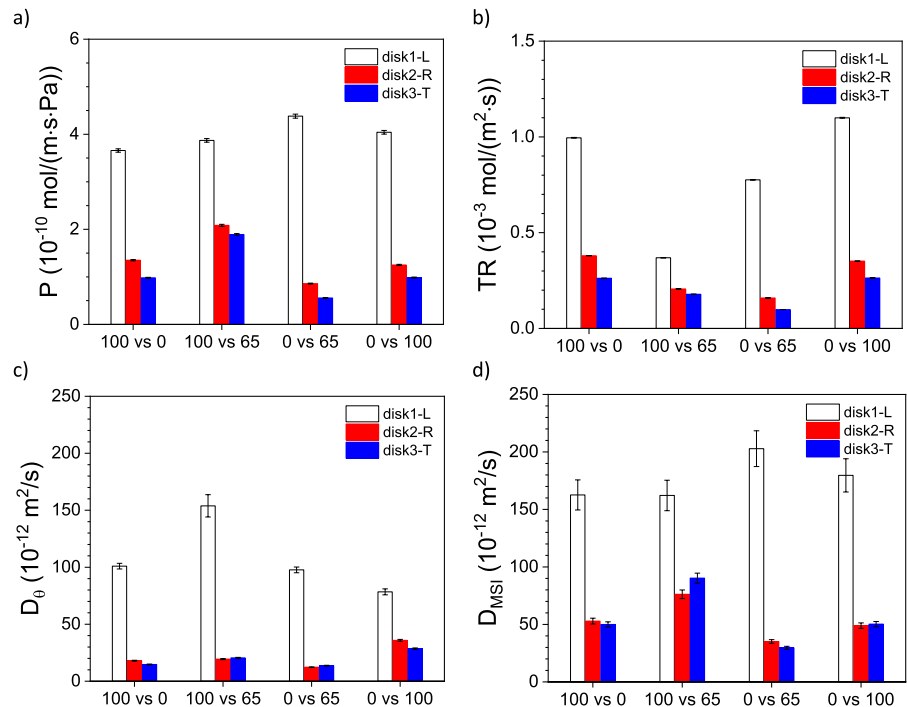
coefficient D and the permeability coefficient P can be calculated. Alternatively, the linear fitting approach was also implemented and similar values for those coming from the exponential-linear approach were obtained for both the mass rate \dot{m} and the lagtime θ (Fig. SI-15) with a minor difference between both methods. The analysis of these curves allows for the determination of the mass rate \dot{m} , the lagtime θ and the lifetime τ , and from those the permeability coefficient P , the diffusion coefficient D_θ ($D_\theta = l^2/6\theta$) and D_τ ($D_\tau = \pi l^2/4\tau$), respectively, together with the sorption coefficient S_θ ($S_\theta = P/D_\theta$) and S_τ ($S_\tau = P/D_\tau$), and the transmission rate (TR) (Table SI-9, SI-10 and SI-11).

While all coefficients should be pressure-dependent, the sorption coefficient is assumed to be a constant that is related to the water–wood interactions—and independent of the sample direction—and, therefore, connected to the water adsorption/desorption capacity of the material. Thus, a comparison was made between the different ways of calculating the sorption coefficient: (i) S_θ and S_τ were obtained from the exponential-linear fitting approach and

combining both the permeability and diffusion coefficients ($S_\theta = P/D_\theta$; $S_\tau = P/D_\tau$); and (ii) S_{MSI} by calculating the sorption coefficient from the MSI profile (S_{MSI} , Eq. B3). The values obtained for the S_θ and S_τ are depending on the sample's direction and on the relative humidity conditions indicating that this approach is not the optimum one for the evaluation of the sorption coefficient. An almost constant value for the sorption coefficient based on the MSI curves was calculated with values of $S_{MSI} \approx 2.1\text{--}2.7 \text{ mol}/(\text{m}^3 \text{ Pa})$ (Fig. SI-16) quite similar to those values averaged from the sorption profiles (Fig. SI-13). Therefore, we assume that this last approach for calculating the sorption coefficient is the closest to reality.

In Fig. 3, a comparison between the three beech disks at different relative humidity conditions in the permeability experiments is shown. In there, it can be identified that the permeability coefficient, the transmission rate and the diffusion coefficient ($P_L = 3.66\text{--}4.38 \times 10^{-10} \text{ mol}/(\text{m s Pa})$, $D_{\theta,L} = 0.78\text{--}1.54 \times 10^{-10} \text{ m}^2/\text{s}$, $TR_L = 3.69\text{--}11.0 \times 10^{-4} \text{ mol}/(\text{m}^2 \text{ s})$) are always higher in the direction parallel

Fig. 3 **a** Permeability coefficient (P), **b** transmission rate (TR), **c** diffusion coefficient obtained from the lagtime value θ (D_θ), and **d** diffusion coefficient obtained from the moisture sorption isotherms (D_{MSI}) for the three beech disks with the water transmission parallel to the longitudinal (L), radial (R), and tangential (T) direction at different relative humidity conditions. Note: in the x-axis, the first value refers to the inner RH-value (cup) and the second one to the outer RH-value (gas flow)



to the longitudinal direction than those from the other two directions ($P_R=0.86\text{--}2.08\times 10^{-10}$ mol/(m s Pa), $D_{\theta,R}=0.12\text{--}0.36\times 10^{-10}$ m²/s, $TR_R=1.59\text{--}3.80\times 10^{-4}$ mol/(m² s); $P_T=0.56\text{--}1.89\times 10^{-10}$ mol/(m s Pa), $D_{\theta,T}=0.14\text{--}0.29\times 10^{-10}$ m²/s, $TR_T=0.99\text{--}2.63\times 10^{-4}$ mol/(m² s)) and with similar values than those published in previous works (Choong et al. 1974; Jinman et al. 1991; Geving et al. 2000; Palanti et al. 2001; Glass 2007; Simo-Tagne et al. 2016). The observed variability within a cutting direction in Fig. 3a is mainly ruled by a gradient in thickness through the sample exposed to different RH-values on both sides of the disk, resulting in one side being more swollen than the other. The diffusion, permeability and sorption coefficients, as well as the transmission rate and fitting parameters of the three beech disks at different relative humidity conditions during the water vapor transmission experiments, are plotted in Fig. SI-16.

In the L-direction, water molecules find the path to move along the sample in a faster way due to the orientation of the xylem structure. The resistance is lowest along the direction of the hollow members of vessels, which in beech wood are relatively evenly distributed, and adjacent axial parenchyma and

vasicentric tracheids—contrary to the perpendicular direction, where only smaller and less prevalent structures like radial parenchyma cells and pits facilitate moisture transport through the wood tissue. Moreover, Fig. 3c and d show the similarity between the values for the diffusion coefficient when calculated from the lagtime θ — $D_\theta=l^2/6\theta$, or by combining both the permeability coefficient and the sorption coefficient (Fig. SI-13)— $D_{MSI}=P/S_{MSI}$.

The relative directional permeability coefficient and diffusion coefficient between the three wood orthotropic directions were also evaluated, as shown in Fig. SI-17. From this evaluation, the L-direction is the one showing the highest permeability coefficient with ratio values ranging from 5.0 to 1.9 (L/R), from 7.9 to 2.0 (L/T), and from 1.5 to 1.1 (T/R). This corresponds to an average L/R ratio value of 3.2 ± 1.4 , an average L/T ratio value of 4.4 ± 2.5 , and an average R/T ratio value of 1.3 ± 0.2 in the relative permeability (P_{rel}) values. Similarly, the average relative diffusion (D_{rel}) values were found to be 5.9 ± 2.7 and 3.6 ± 1.5 (L/R), 6.1 ± 2.2 and 3.9 ± 2.1 (L/T), and 1.1 ± 0.2 and 1.0 ± 0.1 (R/T) from the lagtime values (D_θ), and the MSI experiments (D_{MSI}), respectively.

While it has been found that both the permeability and sorption coefficient could be well-determined and calculated from the DVT experiments, as well as the DVS experiments, some discrepancies appeared in the evaluation of the diffusion coefficient. Figure 4 shows a comparison between the diffusion coefficient values obtained (i) from the DVT experiments—lagtime θ and lifetime τ values -, (ii) from the MSI curves—sorption coefficient S_{MSI} -, and (iii) from the DVS experiments—kinetic constant k . There are similarities between the diffusion coefficients D_θ and D_{MSI} —also with the average \bar{D}_{ads} and \bar{D}_{des} values from the kinetic evaluations—which are in the same order of magnitude, making both DVS and DVT experiments suitable conditions for the evaluation of the diffusion coefficient.

The transmission rate values were plotted as a function of the vapor pressure difference for the three beech disks (Fig. SI-18). The disk with the water transmission parallel to the longitudinal direction (L) showed an almost linear behavior, while a non-linear behavior was observed for the other two directions (R and T)—which could be related to the hysteresis that wood samples show between sorption and desorption processes as already observed somewhere else (Gezici-Koç et al. 2019). Further investigation has to be done in order to confirm such behavior for IUPAC Type IV mesoporous materials like wood (Thommes et al. 2015).

Finally, the moisture capacity M_w of the samples obtained from the exponential-linear fitting approach allows for the estimation of the amount of water adsorbed in the disks during the permeability experiments. This value should correlate to the area under the moisture sorption isotherm between the inner and outer RH-values imposed in the experiments, where M_w is the difference between the steady-state moisture content (the average of the MSI between the boundary conditions) and the initial moisture content. In Fig. 5, this scenario is depicted, where the equilibrium moisture content (EMC) along the thickness of the sample should follow the moisture content isotherm profile. The M_w values obtained for the three beech disks at different relative humidity conditions match well those calculated from the area under the moisture sorption isotherm (Table SI-9, SI-10 and SI-11), with experimental values of $8.2 \pm 0.2\%$, $3.0 \pm 0.1\%$ and $5.3 \pm 0.2\%$ when the inner/outer RH-values were 100% vs 0%, 100% vs 65% and 0% vs 65%, respectively.

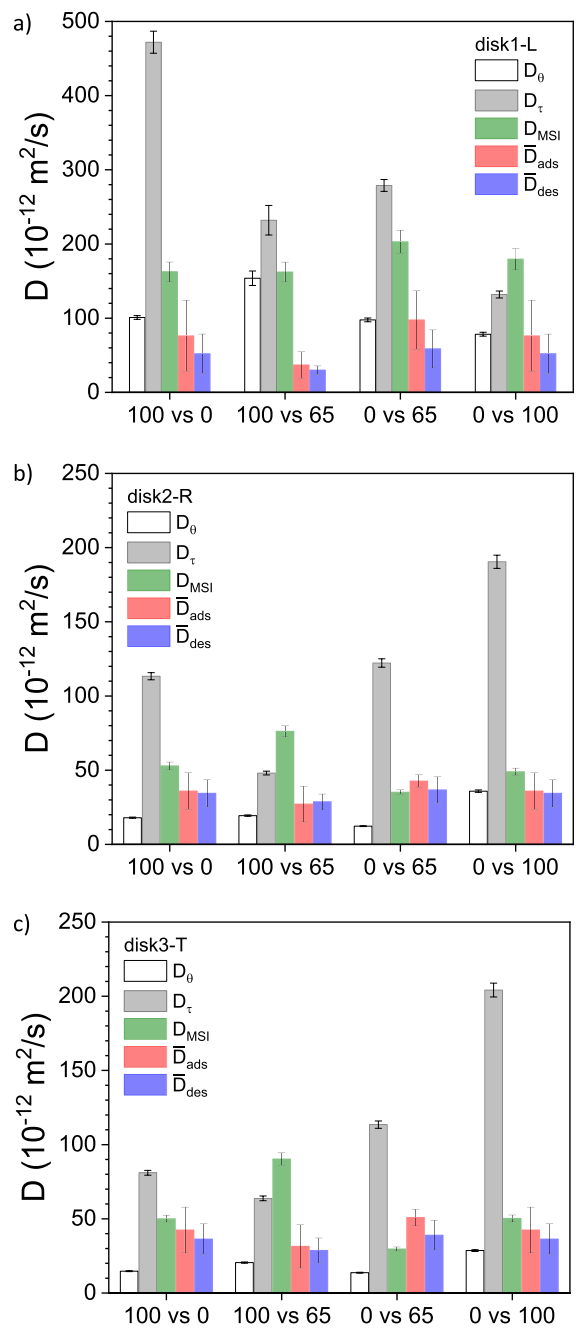


Fig. 4 Comparison of the different diffusion coefficients obtained from the lagtime θ (D_θ) and the lifetime τ (D_τ) values—DVT experiments -, from the sorption coefficient (D_{MSI})—MSI curves -, and from the adsorption and desorption kinetic process (\bar{D}_{ads} and \bar{D}_{des})—DVS experiments—at different relative humidity conditions for the three beech disks: **a** disk1-L, **b** disk2-R, and **c** disk3-T

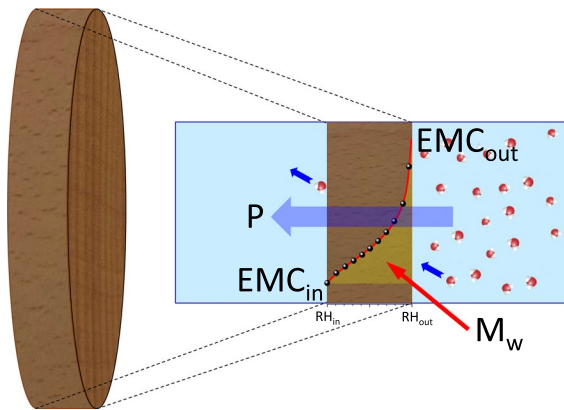


Fig. 5 Moisture content profile along the thickness of a disk after reaching the steady-state following the profile from the moisture sorption isotherm. Water molecules are adsorbed on the surface at the highest RH-value (right), travel through the sample, and are desorbed on the surface at the lowest RH-value (left). The area under the curve (in yellow) corresponds to the moisture capacity of the disk under these conditions

Conclusions

Dynamic Vapor Sorption (DVS) and Dynamic Vapor Transfer (DVT) experiments were performed on beech disks in the three wood orthotropic directions perpendicular to the disk plane in order to evaluate the wood–moisture interactions.

For the DVS experiments, a double stretched exponential (DSE) model was used for the evaluation of the vapor sorption kinetics, and the diffusion coefficient along the three directions was calculated as a function of the RH-value, showing a decrease upon increasing the RH-value. The results show that the directional diffusivity in the longitudinal direction is higher than the one for the tangential and radial direction, with values ranging between 1.52×10^{-10} and 0.11×10^{-10} m²/s, between 0.47×10^{-10} and 0.10×10^{-10} m²/s, and between 0.56×10^{-10} and 0.13×10^{-10} m²/s for the longitudinal, radial and tangential direction, respectively. Moreover, the adsorption diffusivity is higher than the desorption diffusivity due to a change in the conformation of the amorphous water-binding polymers in wood.

Moisture Sorption Isotherm (MSI) curves were constructed from the extrapolated mass ratio values obtained from the DSE fitting of the moisture sorption data. These MSI curves were fitted using the modified Guggenheim-Anderson-de Boer (GAB*)

model and analyzed following a Sorption Site Occupancy (SSO) model. Finally, the sorption coefficient for beech wood was found to be between 2.4 and 3.0 mol/(m³ Pa) and calculated by combining the equilibrium data from the MSI curves, the partial vapor pressure and the volume of the sample as a function of the RH.

DVT experiments allowed for the direct determination of both the diffusion and permeability coefficients and the corresponding transmission rates by applying an exponential-linear model. Diffusivity values range between 1.54×10^{-10} and 0.78×10^{-10} m²/s, between 0.36×10^{-10} and 0.12×10^{-10} m²/s, and between 0.29×10^{-10} and 0.14×10^{-10} m²/s for the longitudinal, radial and tangential direction, respectively, matching quite well the results obtained from the DVS experiments. The calculated permeability coefficients are $P_L = 3.66\text{--}4.38 \times 10^{-10}$ mol/(m s Pa)— $TR_L = 3.69\text{--}11.0 \times 10^{-4}$ mol/(m² s) -, $P_R = 0.86\text{--}2.08 \times 10^{-10}$ mol/(m s Pa)— $TR_R = 1.59\text{--}3.80 \times 10^{-4}$ mol/(m² s) -, and $P_T = 0.56\text{--}1.89 \times 10^{-10}$ mol/(m s Pa)— $TR_T = 0.99\text{--}2.63 \times 10^{-4}$ mol/(m² s)—with similar values than previously reported in the literature using other setups showing that such an experimental approach can definitely be used for evaluating wood–moisture interactions. Further investigations have to be performed using different wood species and chemical treatments.

Acknowledgments Not applicable.

Author contributions All authors contributed to the study's conception and design. Material preparation and data collection were performed by A.S.F. Data analysis was performed by A.S.F. and M.E. The 3D-printed setup for the lagtime experiments was designed and constructed by M.E. The first draft of the manuscript—including figures and tables—was written by A.S.F., and all authors commented on previous versions of the manuscript. All authors read and approved the final manuscript.

Funding Open Access funding enabled and organized by Projekt DEAL. No funding was received for conducting this study.

Availability of data and materials All data are available upon request.

Declarations

Ethics approval and consent to participate Not applicable.

Consent for publication Not applicable.

Competing interests The authors have no relevant financial or non-financial interests to disclose.

Appendix 1: Double stretched exponential function

In this appendix, the comparison between the four exponential models, i.e., the double stretched exponential (DSE), the double exponential (DE) (Zelinka et al. 2021), the single stretched exponential (SSE) (Zeng and Xu 2017) and the single exponential (SE) model are discussed, and the reasons for using the DSE model for fitting the sorption experimental data are given. The SSE model or Weibull (W) model—which is equivalent to a Prony series (Mauro and Mauro 2018) with a finite number of terms—is also compared with the Ritger-Peppas (RP) model for diffusion processes.

The general expression for the four models is the following:

$$\frac{m}{m_{dry}} = \left(\frac{m}{m_{dry}} \right)_{eq} + A_1 e^{-\left(\frac{t-t_0}{\tau_1}\right)^{\beta_1}} + A_2 e^{-\left(\frac{t-t_0}{\tau_2}\right)^{\beta_2}} \quad (9)$$

where m/m_{dry} is the mass ratio with respect to the initial mass of the sample, $(m/m_{dry})_{eq}$ is the mass ratio at the infinite time, A_1 and A_2 , τ_1 and τ_2 , and β_1 and β_2 are the amplitude or moisture step capacity, the lifetime and the stretched exponential factor of each stretched exponential function, respectively. In Table 1, the values corresponding to each model are indicated.

The following four figures (Figs. 6, 7, 8 and 9) show the fitting of some sorption data using the four different exponential models together with the residual analysis. The lifetime τ and the stretched exponential factor β values are also indicated. With these results, it is clear that the DSE model is the best model

Table 1 Values of the amplitude of the second exponential function (A_2) and stretched exponential factor values (β_i) for both exponential functions in Eq. 1 depending on the exponential model used for the analysis of the sorption experiments

	A_2	β_i
DSE	$A_2 \neq 0$	$\beta_i \neq 1$
DE	$A_2 \neq 0$	$\beta_i = 1$
SSE (W)	$A_2 = 0$	$\beta_i \neq 1$
SE	$A_2 = 0$	$\beta_i = 1$

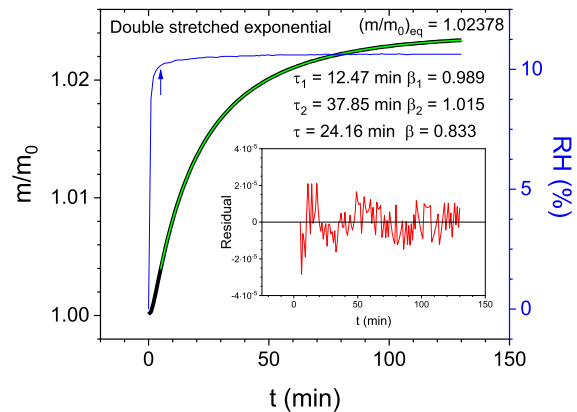


Fig. 6 Analysis of the sorption data using a double stretched exponential (DSE) model. The green curve corresponds to the fitting curve and the blue curve to the relative humidity profile where the starting fitting point is indicated with the blue arrow. Lifetime— τ_1 and τ_2 —and stretched exponential factors— β_1 and β_2 —are indicated together with the equivalent τ and β values corresponding to a Weibull (W) model. The mass ratio at the infinite time— $(m/m_{dry})_{eq}$ —is also indicated. The inset shows the residual analysis of the fitting process

for explaining all experimental data (Thybring et al. 2019) and for the good extrapolation for the evaluation of the mass ratio at the infinite time $(m/m_{dry})_{eq}$.

In order to find out the equivalent τ and β values corresponding to a single stretched exponential

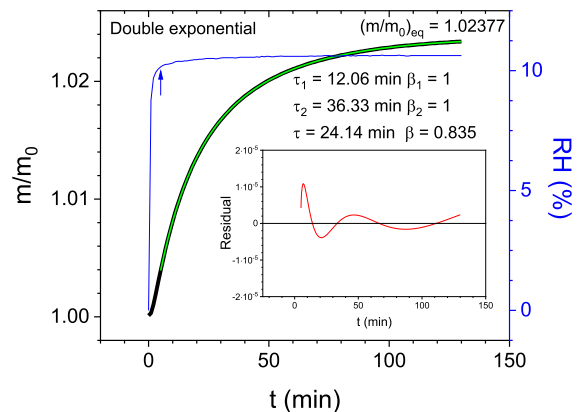


Fig. 7 Analysis of the sorption data using a double exponential (DE) model. The green curve corresponds to the fitting curve and the blue curve to the relative humidity profile where the starting fitting point is indicated with the blue arrow. Lifetime— τ_1 and τ_2 —and stretched exponential factors— β_1 and β_2 —are indicated together with the equivalent τ and β values corresponding to a Weibull (W) model. The mass ratio at the infinite time— $(m/m_{dry})_{eq}$ —is also indicated. The inset shows the residual analysis of the fitting process

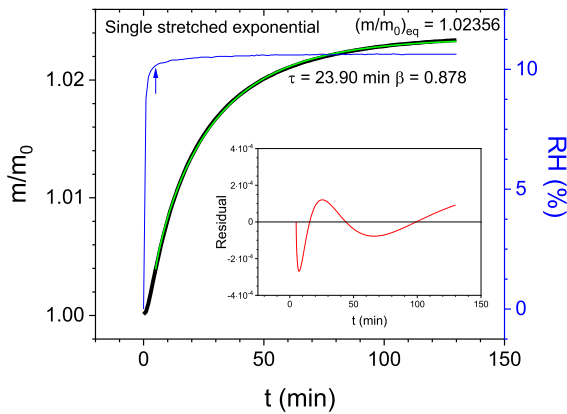


Fig. 8 Analysis of the sorption data using a single stretched exponential (SSE) model. The green curve corresponds to the fitting curve and the blue curve to the relative humidity profile where the starting fitting point is indicated with the blue arrow. The lifetime— τ —and the stretched exponential factor— β —are indicated together with the mass ratio at the infinite time— $(m/m_{dry})_{eq}$. The inset shows the residual analysis of the fitting process

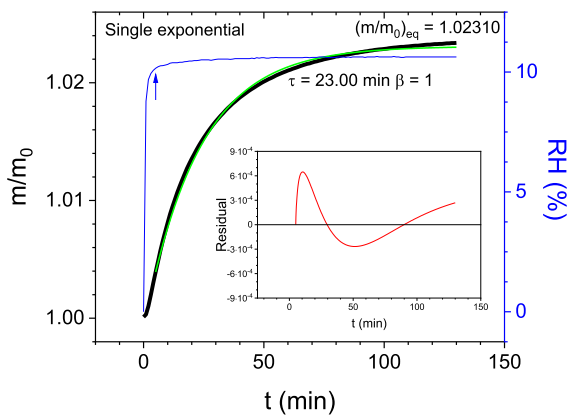


Fig. 9 Analysis of the sorption data using a single exponential (SE) model. The green curve corresponds to the fitting curve and the blue curve to the relative humidity profile where the starting fitting point is indicated with the blue arrow. The lifetime— τ —and the stretched exponential factor— β —are indicated together with the mass ratio at the infinite time— $(m/m_{dry})_{eq}$. The inset shows the residual analysis of the fitting process

(SSE) or Weibull (W) model, the two pairs of parameters coming from a double stretched exponential (DSE) model, i.e., τ_1 - β_1 and τ_2 - β_2 , underwent a minimization of the weighted sum of squares (WSS).

$$WSS = \sum_{n=1}^5 \left(\frac{e^{-n} - f(t_n)}{e^{-n}} \right)^2 \tag{10}$$

where the term e^{-n} corresponds to the reduction of the population when reaching the time equal to n -times the lifetime τ , e.g., for 1τ , 2τ , 3τ , 4τ and 5τ , the population is reduced to 36.79%, 13.53%, 4.98%, 1.83% and 0.67%, respectively, and $f(t_n)$ is a function which includes a normalized version of the DSE model.

$$f(t_n) = \frac{A_1}{A_1 + A_2} e^{-\left(\frac{t_n}{\tau_1}\right)^{\beta_1}} + \frac{A_2}{A_1 + A_2} e^{-\left(\frac{t_n}{\tau_2}\right)^{\beta_2}} \tag{11}$$

As an example, the DSE fitting in Fig. 6 delivered the following values for the fitting parameters A_1 , A_2 , τ_1 , τ_2 , β_1 and β_2 , and the five t_n -values were obtained by applying the minimization process (Table 2).

Once the five t_n -values are obtained, a power-law fitting $t_n = \tau n^{1/\beta}$ is applied, where the pre-factor from the fitting function corresponds to the equivalent lifetime τ and the inverse of the exponent to the stretched exponential factor β of a Weibull (W) model.

Finally, a comparison between the Weibull (W) model and the commonly accepted power-law Ritger-Peppas (RP) model, which is a degeneration of the Weibull model for small $((t-t_0)/\tau)^\beta$ values (Miricioiu et al. 2019) and, therefore, can only be applied to the data covering the 40% of the total amplitude -, was established.

$$\frac{m}{m_{dry}} = \left(\frac{m}{m_{dry}} \right)_{eq} + A \left(\frac{t - t_0}{\tau} \right)^n \tag{12}$$

where m/m_{dry} is the mass ratio with respect to the initial mass of the sample, $(m/m_{dry})_{eq}$ is the mass

Table 2 Values of the fitting parameters (A_1 , A_2 , τ_1 , τ_2 , β_1 and β_2) obtained from Fig. 6 and the corresponding t_n -values from the minimization process

Fitting parameters		t_n -values [min]	
A_1	-0.0085	t_1	24.00
A_2	-0.0113	t_2	55.72
τ_1	12.47 min	t_3	91.44
τ_2	37.85 min	t_4	128.0
β_1	0.989	t_5	164.5
β_2	1.015		

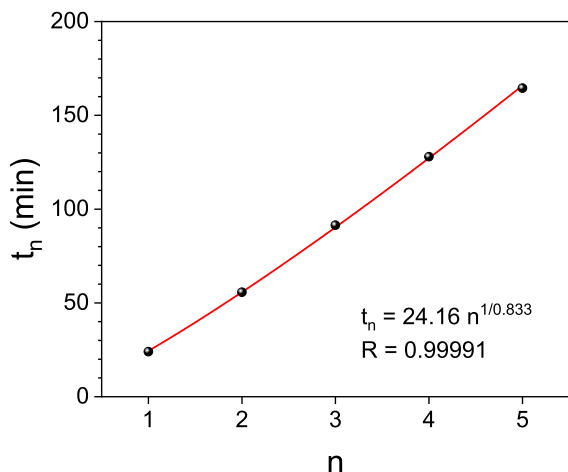


Fig. 10 t_n -values vs. n -values and the corresponding power-law fitting curve for the calculation of the equivalent τ (24.16 min) and β (0.833) values corresponding to a single stretched exponential (SSE) or Weibull (W) model

ratio at the infinite time, A , τ and n are the amplitude, the lifetime and the Ritger-Peppas (RP) exponent. Such an exponent is directly connected to the pseudo-Fickian ($n < 0.5$) (Liu and Neogi 1992), Fickian—or Case I transport—($n = 0.5$) (Boltzmann 1894) and non-Fickian ($0.5 < n < 1.0$) diffusion (Haga 1982), as well as Case II ($n = 1.0$) (Alfrey 1965) and Super Case II ($n > 1.0$) (Jacques et al. 1974) transport (Fig. 10).

In order to find equivalence between both models, single stretched exponential (SSE) or Weibull (W) functions were simulated for different values of the stretched exponential factor β from 0.50 to 1.15 while keeping constant both the amplitude A and the lifetime τ . Figure 11 shows the simulated W functions and in the inset the RP fittings to the simulated W functions values up to the data covering the initial 40% of the total amplitude.

Plotting the RP exponent n vs. the W stretched exponential factor β (Fig. 12) allows for finding the relationship between both parameters. The results allow for classifying the diffusion behavior of the sample as a Fickian ($\beta = 0.586$) and non-Fickian ($0.586 < \beta < 1.146$) diffusion, and Case II ($\beta = 1.146$) and Super Case II ($\beta > 1.146$) transport.

Moreover, this correlation also allows for the calculation of the W kinetic constants k_W or the

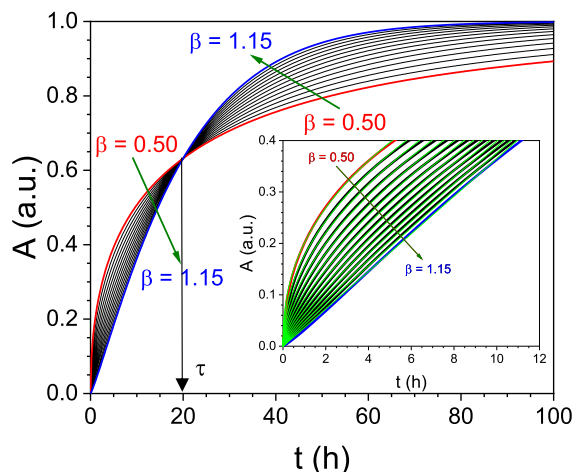


Fig. 11 Single stretched exponential (SSE) or Weibull (W) function simulations with the stretched exponential factor β ranging from 0.50 to 1.15. The inset shows the Ritger-Peppas (RP) fitting function—green curves—to the Weibull (W) simulated points—black curves—up to the initial 40% of the total amplitude ($A = 0.4$)

corresponding lifetime τ_W from the corresponding RP parameters (Fig. 13).

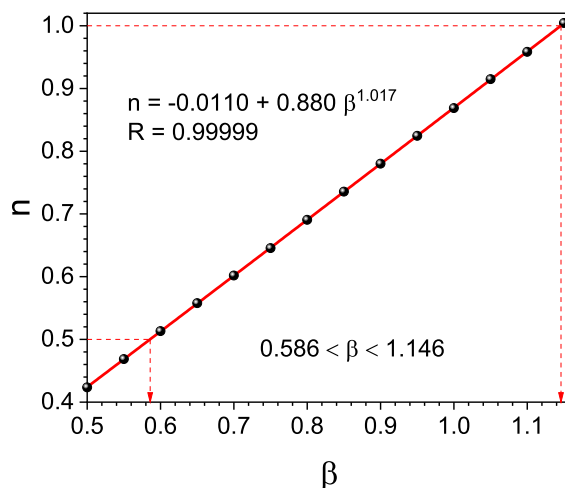


Fig. 12 Correlation between the Weibull (W) stretched exponential factor β and the Ritger-Peppas (RP) exponent n showing the non-Fickian diffusion ($0.5 < n < 1.0$) applies to values between $0.586 < \beta < 1.146$

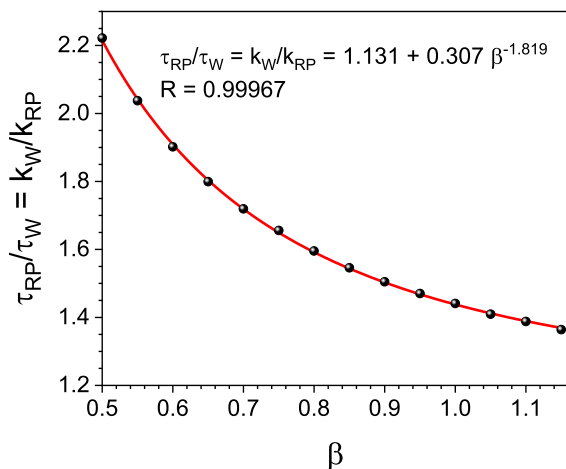


Fig. 13 Relation between the kinetic constant from the Weibull (W) model and the Ritger-Peppas (RP) model as a function of the stretched exponential factor β

Appendix 2: Fitting moisture sorption isotherms

In this appendix, the comparison between samples based on their moisture sorption isotherms is detailed using the modified Sorption Site Occupancy (SSO) model based on the statistical occupancy of accessible sorption sites in the sample (Freundlich 1906). This model assumes that proton-active moieties, i.e., hydroxyl groups in the lignocellulosic polymers, are responsible for binding water molecules during the sorption process that follows a power-law model (Willems 2014,2015).

$$M_{SSO} = M_{SSO}^0 a_w^n \quad (13)$$

where M_{SSO} is the moisture capacity corresponding to the bound water molecules to the sorption sites as a function of the water activity, M_{SSO}^0 is the maximum amount of bound water, n is the exponent, and a_w is the water activity— $a_w = RH/100$.

Firstly, and for purely interpolation purposes, the modified Guggenheim-Anderson-de Boer (GAB*) (Viollaz and Rovedo 1999; Sandoval et al. 2011) model was implemented. From the fitting of the sorption steps and using the DSE model, the mass ratio at the infinite time $(m/m_{dry})_{eq}$ was obtained. Then, the relative increment $\Delta m/m_{dry}$ —the moisture content—was calculated ($\Delta m/m_{dry} = (m/m_{dry})_{eq} - 1$). The corresponding moisture sorption isotherms were constructed by plotting the $\Delta m/m_{dry}$ values

as a function of the relative humidity RH or water activity a_w .

The GAB* model has the following expression:

$$\frac{\Delta m}{m_{dry}} = \frac{M_0 C K a_w}{(1 - K a_w)(1 + (C - 1) K a_w)} + \frac{M_0 C K N a_w^2}{(1 - K a_w)(1 - a_w)} \quad (14)$$

where M_0 , C , K and N are the fitting parameters and a_w is the water activity.

Secondly, the SSO model was implemented by calculating the tangent to the local minimum (a_w^*) in the log–log representation of the moisture sorption isotherm from the GAB* model, allowing for the calculation of the moisture capacity related to the bound water molecules (M_{SSO}).

Finally, the moisture capacity corresponding to the non-bound water molecules in the cell wall was evaluated by the difference between the fitted GAB* (Eq. B2) curve and the SSO curve (Eq. B1). This moisture content corresponds to the water molecules in charge of softening the cell wall and, therefore, swelling the wood structure (Vrentas and Vrentas 1991; Berthold et al. 1996).

The sorption coefficient S can be calculated from the moisture isotherm.

$$S(RH) = \frac{C}{p} = \frac{\left(\frac{\Delta m}{m_{dry}}\right)\rho}{p m_w} = \frac{\left[\left(\frac{\Delta m}{m_{dry}}\right)^2 + \left(\frac{\Delta m}{m_{dry}}\right)\right] m_{dry}}{p V m_w} \quad (15)$$

where m_{dry} is the mass of the sample at 0% RH, p , ρ and V are the water partial pressure, the density and the volume of the sample at different relative humidity values, respectively, and m_w is the molar mass of water (18.01528 g/mol). Note that C is the moisture concentration in the sample following Henry's law, and $p = 28.62$ RH.

Open Access This article is licensed under a Creative Commons Attribution 4.0 International License, which permits use, sharing, adaptation, distribution and reproduction in any medium or format, as long as you give appropriate credit to the original author(s) and the source, provide a link to the Creative Commons licence, and indicate if changes were made. The images or other third party material in this article are included in the article's Creative Commons licence, unless indicated otherwise in a credit line to the material. If material is not included in the article's Creative Commons licence and your intended use is not permitted by statutory regulation or exceeds the permitted use, you will need to obtain permission directly from the copyright holder. To view a copy of this licence, visit <http://creativecommons.org/licenses/by/4.0/>.

References

- Alfrey T (1965) Glassy polymer diffusion is often tractable. *Chem Eng News* 43:64–65
- Al-Ismaily M, Wijmans JG, Kruczek B (2012) A shortcut method for faster determination of permeability coefficient from time lag experiments. *J Membr Sci* 423–424:165–174
- Amini-Fazl MS, Mobedi H (2020) Investigation of mathematical models based on diffusion control release for paclitaxel from in-situ forming PLGA microspheres containing HSA microparticles. *Mater Technol* 35:50–59
- Anderson RB (1946) Modifications of the Brunauer, Emmett and Teller equation. *J Am Chem Soc* 68:686–691
- Avramidis S, Siau JF (1987) An investigation of the external and internal resistance to moisture diffusion in wood. *Wood Sci Technol* 21:249–256
- Babbitt JD (1950) On the differential equations of diffusion. *Can J Res A* 28:449–474
- Basu S, Shivhare US, Mujumdar AS (2006) Models for sorption isotherms for foods: a review. *Dry Technol* 24:917–930
- Berthold J, Rinaudo M, Salmén L (1996) Association of water to polar groups—estimations by an adsorption model for lignocellulosic materials. *Colloid Surf A* 112:117–129
- Boltzmann L (1894) Zur Integration der Diffusionsgleichung bei variabeln Diffusionscoefficienten. *Alln Phys Chem* 53:959–964
- Burnett DJ, Garcia AR, Thielmann F (2006) Measuring moisture sorption and diffusion kinetics on proton exchange membranes using a gravimetric vapor sorption apparatus. *J Power Sources* 160:426–430
- Choong ET, Fogg PJ (1972) Variation in permeability and treatability in shortleaf pine and yellow poplar. *Wood Fiber Sci* 1972:2–12
- Choong ET, Tesoro FO, Manwiller FG (1974) Permeability of twenty-two small diameter hardwoods growing on southern pine sites. *Wood Fiber Sci* 1974:91–101
- Crank J (1975) *The Mathematics of Diffusion*, 2nd edn. Clarendon Press, Oxford
- Freundlich HMF (1906) On the adsorption in solutions. *Z Phys Chem* A57:385–470
- Fuoco A, Monteleone M, Esposito E, Bruno R, Ferrando-Soria J, Pardo E, Armentano D, Jansen JC (2020) Gas transport in mixed matrix membranes: two methods for time lag determination. *Computation* 8:28
- Geving S, Time B, Hovde PJ (2000) Water vapour permeability and hygroscopic sorption curves for various building materials. *Proceedings of the Heat and Moisture Transfer in Building Conference 2000*:117–122
- Gezici-Koç Ö, Erich SJF, Huinink HP, van der Ven LGJ, Adan OCG (2017) Bound and free water distribution in wood during water uptake and drying as measured by 1D magnetic resonance imaging. *Cellulose* 24:535–553
- Gezici-Koç Ö, Erich SJF, Huinink HP, van der Ven LGJ, Adan OCG (2019) Moisture content of the coating determines the water permeability as measured by 1D magnetic resonance imaging. *Prog Org Coat* 130:114–123
- Glass SV, Boardman CR, Thybringer EE, Zelinka SL (2018) Quantifying and reducing errors in equilibrium moisture content measurements with dynamic vapor sorption (DVS) experiments. *Wood Sci Technol* 52:909–927
- Glass SV (2007) Measurements of moisture transport in wood-based materials under isothermal and non-isothermal conditions. *Proceedings ASHRAE*, pp 1–13
- Grönquist P, Frey M, Keplinger T, Burgert I (2019) Mesoporosity of delignified wood investigated by water vapor sorption. *ACS Omega* 4:12425–12431
- Haga T (1982) Structural considerations in Case II swelling of crystalline poly(ethylene terephthalate). *J Appl Polym Sci* 27:2653–2661
- Hansmann C, Gindl W, Wimmer R, Teischinger A (2002) Permeability of wood—a review. *Wood Res* 4:1–16
- ISO 12572 Hygrothermal performance of building materials and products—Determination of water vapour transmission properties—Cup method
- Jacques CHM, Hopfenberg HB, Stannett VT (1974) *Permeability of plastic films and coatings to vapors and liquids*. Plenum
- Jinman W, Chengyue D, Yixing L (1991) *Wood Permeability* J Northeast for Univ 2:91–97
- Kollmann F (1963) *Zur Theorie Der Sorption* Forsch Ing-Wes 29:33–41
- Lehringer C, Richter K, Schwarze FW, Militz H (2009) A review on promising approaches for liquid permeability improvement in softwoods. *Wood Fiber Sci* 41:373–385
- Liu CPA, Neogi P (1992) Sorption of methylene chloride in semicrystalline polyethylene terephthalate. *J Macromol Sci Phys B* 31:265–279
- Majka J, Rogoziński T, Olek W (2022) Sorption and diffusion properties of untreated and thermally modified beech wood dust. *Wood Sci Technol* 56:7–23
- Mauro JC, Mauro YZ (2018) On the Prony series representation of stretched exponential relaxation. *Phys a: Stat Mech Appl* 506:75–87
- Mircioiu C, Voicu V, Anuta V, Tudose A, Celia C, Paolino D, Fresta M, Sandulovici R, Mircioiu I (2019) Mathematical modeling of release kinetics from supramolecular drug delivery systems. *Pharmaceutics* 11:140
- Negrini R, Sánchez-Ferrer A, Mezzenga R (2014) Influence of electrostatic interactions on the release of charged molecules from lipid cubic phases. *Langmuir* 30:4280–4288
- Nelson RM (1983) A model for sorption of water vapor by cellulosic materials. *Wood Fiber Sci* 1933:8–12
- Neogi P (1996) *Diffusion in Polymers*. Marcel Dekker
- Olek W, Perré P, Weres J (2005) Inverse analysis of the transient bound water diffusion in wood. *Holzforschung* 59:38–45
- Palanti S, Berti S, Becarelli S, Martena F (2001) A simple testing method for the measurement of the water vapour transmission of coated wood longitudinal and tangential to grain direction. *Holzforschung* 55:328–331
- Panigrahi S, Kumar S, Panda S, Borkataki S (2018) Effect of permeability on primary processing of wood. *J Pharmacogn Phytochem* 7:2593–2598
- Peleg M (1988) An empirical model for the description of moisture sorption curves. *J Food Sci* 53:1216–1219
- Piringer OG, Baner AL (2000) *Plastic packaging materials for food barrier function, mass transport, quality assurance, and legislation*. Wiley-VCH

- Raucher D, Sefcik MD (1983) Sorption and transport in glassy polymers. *ACS Symp Ser* 223:111–124
- Ritger PL, Peppas NA (1987) A simple equation for description of solute release I. Fickian and non-Fickian release from non-swelling devices in the form of slabs, spheres, cylinders or discs. *J Control Release* 5:23–36
- Ross RJ (2010) *Wood Handbook - Wood as an Engineering Material*. Forest Products Laboratory, USDA Forest Service, FPL-GTR-190
- Sandoval AJ, Barreiro JA, Müller AJ (2011) Determination of moisture adsorption isotherms of rice flour using a dynamic vapor sorption technique. *Interciencia* 36:848–852
- Siau JF (1984) *Transport processes in wood*. Springer, Berlin
- Siepmann J, Peppas NA (2011) Higuchi equation: derivation, applications, use and misuse. *Int J Pharm* 418:6–12
- Simo-Tagne M, Rémond R, Rogaume Y, Zoulalian A, Perré P (2016) Characterization of sorption behavior and mass transfer properties of four central africa tropical woods: ayous, sapele, frake, lotofa. *Maderas Cienc Technol* 18:207–226
- Skaar C (1988) *Wood-water relations*. Springer, Berlin
- Thommes M, Kaneko K, Neimark AV, Olivier JP, Rodriguez-Reinoso F, Rouquerol J, Sing KSW (2015) Physisorption of gases, with special reference to the evaluation of surface area and pore size distribution. *Pure Appl Chem* 87:1051–1069
- Thorell A, Wadsö L (2018) Determination of external mass transfer coefficients in dynamic sorption (DVS) measurements. *Dry Technol* 40:332–340
- Thybring EE, Glass SV, Zelinka SL (2019) Kinetics of water vapor sorption in wood cell walls: state of the art and research needs. *Forests* 10:704
- Thybring EE, Piqueras S, Tarmian A, Burgert I (2020) Water accessibility to hydroxyls confined in solid wood cell walls. *Cellulose* 27:5617–5627
- Thybring EE, Boardman CR, Zelinka SL, Glass SV (2021) Common sorption isotherm models are not physically valid for water in wood. *Colloids Surf A Physicochem Eng Asp* 627:127214
- Viollaz PE, Rovedo CO (1999) Equilibrium sorption isotherms and thermodynamic properties of starch and gluten. *J Food Eng* 40:287–292
- Vrentas JS, Vrentas CM (1991) Sorption in glassy polymers. *Macromolecules* 24:2404–2412
- Vrentas JS, Vrentas CM (1996) Hysteresis effects for sorption in glassy polymers. *Macromolecules* 29:4391–4396
- Weibull W (1951) A statistical distribution function of wide applicability. *J Appl Mech* 18:293–297
- Willems W (2014) The water vapor sorption mechanism and its hysteresis in wood: the water/void mixture postulate. *J Wood Sci Technol* 48:499–518
- Willems W (2015) A critical review of the multilayer sorption models and comparison with the sorption site occupancy (SSO) model for wood moisture sorption isotherm analysis. *Holzforchung* 69:67–75
- Xiao C, Shi P, Yan W, Chen L, Qian L, Kim SH (2019) Thickness and structure of adsorbed water layer and effects on adhesion and friction at nanoasperity contact. *Colloids Interfaces* 3:55
- Yu X, Schmidt AR, Bello-Perez LA, Schmidt SJ (2008) Determination of the bulk moisture diffusion coefficient for corn starch using an automated water sorption instrument. *J Agric Food Chem* 56:50–58
- Zelinka SL, Thybring EE, Glass SV (2021) Interpreting dynamic vapor sorption (DVS) measurements: why wood science needs to hit the reset button. *Proceedings of the World Conference on Timber Engineering EPFT0101*
- Zeng Q, Xu S (2017) A two-parameter stretched exponential function for dynamic water vapor sorption of cement-based porous materials. *Mater Struct* 50:128

Publisher's Note Springer Nature remains neutral with regard to jurisdictional claims in published maps and institutional affiliations.